INTERNATIONAL JOURNAL OF AUTOMOTIVE SCIENCE AND TECHNOLOGY

2023, VOL. 7, NO:1, 44-53 www.ijastech.org e-ISSN: 2587-0963

An experimental examination of the effect of temperature distributions in different welding sorting of the part transmitting thrust in front loader of tractors by means of MAG method on displacements

Haluk Güneş[1], Salih Özdel

0000-0002-0915-0924, 0000-0003-0345-2419

[1] *Department of Motor Vehicles and Transportation Technologies, Tavsanlı Vocational School, Dumlupinar University, Kutahya, 43300, Turkey*

Abstract

In this study, temperatures of samples welded by 3 different welding sorting has been measured and displacements occurring on the part after wielding have been determined and an experimental comparison has been made in this regard. The welded part belongs to the front loader used in tractors. Material of the model is S355j2+N. In the experimental study, 3 samples have been welded for each process. In Process 1, welding lines have been observed outside to inside, in Process 2 inside to outside, and in Process 3 from right to left. For all parts, welding parameters and welding speed have been fixed. Welding manufacture and cooling processes have lasted 3000 seconds in total. 4 points have been determined in order to measure the temperature of the part during the experiment. For determination of displacement amount, sample parts have been measured by means of 3-dimensional laser measuring device before and after welding. When results of experiment are examined, it has been observed that temperatures curves are similar in processes no. 1 and 3; and the process has been completed by lower temperature in process no. 2. The highest temperatures measured in processes 1, 2 and 3 are respectively as 380ºC, 272ºC ve 310ºC. Displacements of circular and cylindric points are respectively as 2.17 mm, 1.22 mm, 2.12mm. Maximum displacements of the surfaces are as 0.40 mm, 0.41 mm, 0.80 mm for process 1; as 0.10 mm, 0.28 mm, 0.83 mm for process 2; and as 0.71 mm 0.77 mm 1.39 mm for process 2. It has been concluded that process no. 2 has lower temperatures and less displacements. Less amount of displacement or distortion provides use of parts without applying correction afterwards, and eliminates surplus workmanship and time loss.

Keywords: Distortion analysis; Gas metal arc welding; Heat transfer; Temperature distribution; Vehicle design.

Research Article

https://doi.org/10.30939/ijastech..1231161

Received 08.01.2023
Revised 30.01.2023
Accepted 12.02.2023

* Corresponding author

Haluk Güneş

haluk.gunes@dpu.edu.tr

Address: Department of Motor Vehicles and Transportation Technologies, Tavsanlı Vocational School, Dumlupinar University, Kutahya, Turkey

Tel:+902746146778

1. Introduction

During welding processes carried out by means of gas metal arc, which is a frequently used welding method in the industry, very high and non-homogenous heat inputs occur. In the stage following the welding process, cooling of the welded area and the rest of material last for different periods of time. Such situation results in residual stress and distortions on the base metal. Even some parts become unusable. If no precaution is taken, correction of such negative impacts becomes overcostly and takes time. In today's industry, efficient use of energy and waste energy recovery systems have gained importance [1]. Parts defects that may occur during the welding process lead to inefficient energy consumption. Component defects caused by residual stresses can be minimized by means of proper welding sorting

Nart and Çelik, in their study, have suggested a new practical approach by using certain modifications and double ellipsoid model in order to achieve the proper shape of weld pool. Temperature distribution and residual stress have been estimated by means of finite element method via ABAQUS software. It has been observed that the number of conductivities in fusion area improves estimation of thermal move, that the results become closer to the experimental results as dimensions of mesh get smaller, and experimental results of the analysis are satisfactory [2]. Yavuz et al., in

one of their studies, have aimed to determine beforehand the mechanical properties of HAZ region, whose mechanical properties are not known exactly and which occur near to the weld pool during welding of unalloyed structure steels with st52-e quality, by means of finite elements method. Ansys package programme has been preferred among FEM programmes. Submerged arc welding method has been used, which has larger HAZ region when compared to other welding methods. During welding process, ESAB LAW 1000 DC submerged arc welding machine has been used. Tensile test samples have been derived in parallel to weld bead from the welded workpiece. As a result of the study, thermal and mechanical analyses results of the workpiece have been obtained [3]. Kaya, in his study, has compared consistency between experimental hook results of the welded steel material with st-37 quality and the numeric results. Workpiece has been connected by means of MAG, TIG and submerged arc welding methods, and micro structures have been examined under the microscope. Modelling has been realised in computer-aided environment by using date such as mechanical properties and welding parameters of the material as derived from the results obtained by means of experimental examination of the parts. ABAQUS software has been selected to apply finite elements method. It has been observed that analysis results and experimental results of the solved mathematical model are consistent [4]. Wu et al. present simulation of a butt-welded workpiece, welded by fusion, solved by means of finite element method. In order to simulate 3-dimensional welding process modelled as one-run, 2-dimensional finite elements method analysis has been used. In order for finite elements solution, ANSYS has been used, while temporary thermal analysis has been applied to obtain heat distributions. It has been assumed that HAZ, whose mechanical properties are not known exactly, and the welding metal have the same properties with the workpiece. They have proved that results of analysis are consistent with the experimental results [5]. Wen et al. have modelled a multistranded submerged arc welding process by using a finite element package ABAQUS for general purposes. Production of thick-walled pipe weld with 2D and 3D models is simulated. Results, obtained by considering and non-considering residual stress occurring in pre-welding process, have been compared to experimental data. It has been detected that distortions, occurring as a result of welding process, can be decreased by means of process improvements. It has been observed that future processes can be improved by means of finite elements method [6]. Gunaraj and Murugan have developed a mathematical model in order to examine the effects of process variants and heat inputs upon requirement for selecting conditions to provide predictable and repeatable weld-bead, which is critical to acquire high quality. In such study, colour metallography technique and response surface methodology have been used. It has been observed that heat input and feed rate have positive impact on HAZ; however, it has been stated that welding speed has negative impact on HAZ properties. It has been observed in the sample that the increase in voltage results in increase in the grain size, and maximum HAZ width has been obtained at minimum welding progress and wire feed speed [7]. Song et al. Carried out a study in order to evaluate sensitivity of thermomechanical responses against the changes in parameters of various materials of welded connections. Thermoplastic material model, independent from speed, with low deformation and having thermal material properties, has been adopted. Connection of stainless-steel AL-6XN by corner weld has been examined [8]. In their study, they have carried out experiment and analyses in order to evaluate geometrical parameters of double ellipsoidal heat source model of John Goldak. For welding simulation, the commercial software Sysweld, found prevalently as FEA means, has been selected. They have carried out the experimental study on AS 3678-250 with the size of 200x100x12 mm3. Macro images of the obtained results have been examined and validation has been made [9]. Piekarska and Kubiak have studied on mathematical modelling and numerical analysis in order to determine thermal factors, which are highly impossible to be determined experimentally in laser weld and laser arc weld, and the parameters to be used in production. It has been observed that laser arc weld enables to double the progress speed when compared to the laser weld, that laser arc is better in longer workpieces, that negative impacts in laser arc weld are less in HAZ region when compared to laser weld due to cooling speeds. The mathematical modelling formed has shown compliance to the experimental results [10].

Nezamdost et al., in one of their studies, provide information about a numerical and experimental research in order to comprehend and improve computer methods in implementation of Goldak model to estimate thermal distribution of APIX65 pipe line steel at submerged arc welding. It has been aimed to control micro structures and mechanical properties. The analysis has been carried out by ABAQUS programme as 2D and 3D. It has been observed that residual stress of analyses can be used effectively in prediction and 2D analysis is much more advantageous in terms of time and cost when compared to 3D analysis. It has been observed that experimental results are in compliance with the analysis [11].

Fachinotti et al. have formed a series of walls from alloy by using Shaped Metal Deposition (SMD) welding machine, and analysed the heat transfer problem occurring during layer deposition at every case. Samples have been formed by various process parameters (number of layers, height of layer, wire feed speed, motion speed, heat input, etc.) and Wall dimensions. A finite element model has been created in order for thermal analysis of such deposition process. Such numerical model has foreseen a real-like welding [12]. Pu et al. have studied on three different modelling in order to search residual stress and distortions occurring after welding process: the model with heat source moving at multiple-run butt-welding applied to high tensile Q345 steel; the model called as incident heat source; and the model with intense mesh network. Mechanical properties of welding metal and workpiece as well as yield stress differences have been taken into consideration. In order to see residual stress and deformation amounts, perforation and three-coordinate measurement system have been used. It has been observed that experimental results of moving heat source can be estimated better; that incident heat source model can foresee reasonable result only for residual stress; that the model with intense mesh network can potentially estimate residual stress in thick

workpieces [13]. Knoedel et al., in their research examining practical aspects of welding simulation, have analysed a simple but effective engineering approach for calculation of residual stress during welding process by means of finite elements method increased currently. ANSYS software has been used for finite element analysis. One-run welding has been made by HT-steel and S355J2. The results obtained have been compared to the experimental results in the literature and it has been observed that they are consistent [14]. Yadav et al. have carried out submerged arc welding experiments on low carbon steels. They have examined HAZ area deformations and weld-bead. They have carried out analysis in order to calculate fluid flow and heat transfer by modelling the heat source. Model of three-dimensional oval heat source has been obtained from experimental weld geometry. In their study, they have put forward that there are micro structural examinations on the samples, significant grain growth in the heat-affected area, and thin and equiaxed grains in fusion area [15]. Podder et al, in their study, have dealt with double ellipsoidal heat source model at submerged welding of low carbon steels between 6- and 16-mm. Arc efficiency has been accepted as 0.9. 1200 A constant current has been applied during welding; the workpiece has been welded by using copper-covered electrode with a diameter of 4 mm. In this study, parts with thicknesses of 6, 8, 10, 12 and 16 mm have been used. The temperature at upper and lower surfaces have been measured by thermos-couples. Two thermos-couples have been positioned upper and lower parts of the place and 25 mm away from the weld-bead. Regression equation has been formed by measuring related parameters of weld pools and by means of experiments. Model and analysis have produced consistent results [16].

Minh and Phu, in one of their studies, have examined deformations on the welded material by simulation and experiment. They modelled a connected joint geometry structure by using Simufact welding software based on thermo-elastic-plastic approach, and have made simulations. In order to compare the results of simulation, digital gas metal arc welding has been used and experiments have been made with three different welding sorting and put forward deformation amounts of them. The first welding sorting has been made from left to right; the second outside to inside; and the third from inside to outside. In such experiments, low carbon steel AISI 1005 has been selected as base metal. When the results are examined, it has been determined that thermo-elastic-plastic 3B FEM analysis show compliance with experimental results, and "inside to outside" welding sorting causes less deterioration when compared to the "outside to inside" sorting. Moreover, deformation profiles are the same in three processes. However, deformation values change significantly. The biggest deformation occurs in process no. 1; it decreases significantly in processes no. 2 and 3 [17]. Zhang et al. have examined welded manufacturing of vacuum reservoirs (VV) of Chinese Fusion Engineering Testing Reactor (CFETR) which have close tolerance. They have analysed 1/32 scale model they formed in ABAQUS package programme. During the analysis, three different TIG weld-beads have been simulated. It has shown that the main welding stress have occurred in welding area, and maximum deterioration in the Shell close to the welding connection between internal and lower parts. Finite elements model has included 90.280 mesh and 135.988 nodes. While the internal segment, upper segment and lower segment have deteriorated vertically towards inside of the Shell; central segment (PS3) has deteriorated vertically towards outside of the Shell. An optimised welding sorting has been obtained and could be applied to practical installation of 1/32 VV model [18].

In this study, the objective is to put forward distortions, temperature distributions and effective stresses of a part produced from S355J2+N and to be connected by MAG welding method. Related part is an element transmitting thrust in front loader of tractors and it is shown in Figure 1. For experiments, 3 welding sorting has been determined and 3 sample parts have been produced for each process.

Fig. 1. The part transmitting thrust in front loader of tractors

In Table 1, mechanical and chemical properties of the samples to be welded and the welding wire are shown. Here, while selecting the materials, technical compliance with the areas to be used in tractors have been taken into consideration. SG-2 welding wire has been used.

Table 1. Chemical and mechanical properties of steel and welding wire.

S355J2+N Steel	Chemical properties	C	Si	Mn	P	S	Cr	Ni	Al	Cu	Cev
		%									
		0.20	0.24	0,40	0,010	0,005	0,13	0,12	-	0,20	-
	Mechanical properties	Yield strength		Tensile strength		Notch impact strength (-20°C)				Elongation %	
		N/mm2				J				%	
		365		532		27				32	
SG-2 Welding wire	Chemical properties	C	Si	Mn	P	S	Cr	Ni	Al	Cu	Cev
		%									
		0,08	0,85	1,45	-	-	-	-	-	-	
	Mechanical properties	Yield strength		Tensile strength		Notch impact strength (-30°C)				Elongation %	
		N/mm^2				J				%	
		420		500 - 640		47				22	

During welding process, HB-105 mixed gas at M14 standards produced for MAG welding has been used. Chemical formula of the gas includes 95% Ar, 3% CO_2 and 2 %O_2. Welding parameters have been fixed for all processes. Welding flow and voltage are respectively 245A and 26.2V. Progress rate is 0.0057 m/s in planar welding areas; and 0.008 m/s in circular areas.

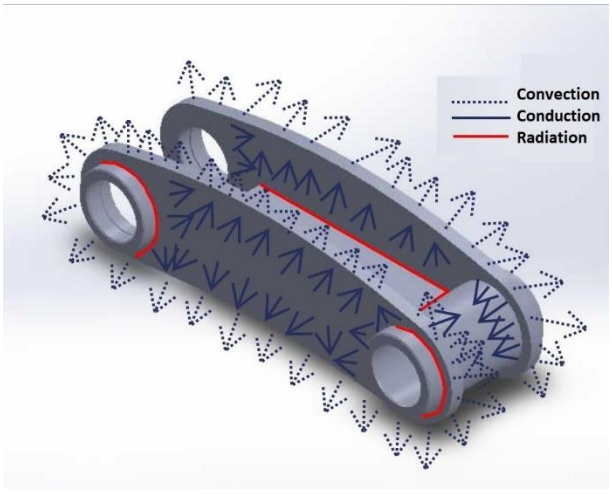

Fig. 2. Heat transfer points on the workpiece

In Figure 2, areas on which heat transfer has realised during welding on the workpiece are shown. In this part, heat transfer is realised by 3 ways as radiation, convetion and conduction. Movement directions in the figure have been shown symbolically. Equation 1 is given in the simplest form of heat transfer by radiation [19].

$$\dot{Q}_{rad} = \varepsilon\sigma A_s(T_s^4 - T_{surr}^4) \quad (1)$$

Here, $\dot{Q}_{rad}$ is the amount of heat transfer by radiation (W), T_S surface temperature (K), T_{Surr} ambient temperature (K), A_s surface area (m^2) ε emission coefficient (emissivity), σ Stefan-Boltzmann constant (5.67×10^{-8} Wm^{-2} K^{-4}), α is the absorbance ratio.

Heat transfer by convection is the transfer of energy from solid surfaces to liquid or gas. It can be calculated by Equation 2 [20].

$$\dot{Q}_{conv} = hA_S(T_s - T_\infty) \quad (2)$$

Here, $\dot{Q}_{conv}$ is the convection heat transfer amount (W), h is the heat transfer coefficient ($Wm^{-2}K^{-1}$), A_s is the surface area (m^2), T_s is the surface temperature (K), T_∞ is the ambient temperature (K).

In conduction heat transfer, energy is transferred from the higher-energy one to the less-energy one of the interacting neighboring particles, and it can be expressed by equation 3 [20].

$$\dot{Q}_{cond} = -kA\frac{\Delta T}{\Delta X} = -kA\frac{dT}{dx} \quad (3)$$

$\dot{Q}_{cond}$ amount of heat transfer by conduction (W), A area (m^2), k thermal conductivity coefficient (Wm^{-1} K^{-1}) dT temperature difference (K), dx thickness (t). The heat inputs of the welding zone can be expressed with the following equations [20].

$$P = E.I \quad (4)$$

$$Q = f\frac{P.60}{v.1000} \quad (5)$$

$$Q = f\frac{E.I.60}{v.1000} \quad (6)$$

Here Q is the amount of heat per unit length of the welding pass (kJm^{-1}), P is the total energy taken from the heat source (W), E is the arc voltage (V), I is the arc current (A) f is the heat conduction efficiency. This value is about 0.8 in arc welding with covered electrodes. v is the welding speed (m/min).

2. Material and Method

Welding robot used is the **KR 8 R2100-2 arc HW** model of **KUKA** brand, which can be seen in Figure 3 while being programmed. Welding paths are programmed by using handheld terminal by the operator. Technical properties of KR 8 R2100-2 arc HW model have been shown in Table 2.

In the experiment, TPS/i 320 A model of Fronious brand has been used as gas arc welding machine integrated with KUKA robot. Technical properties of TPS/i 320 A model have been given in Table 2.

Fig. 3. Welding robot

Table 2. Technical properties of KR 8 R2100-2 arc HW ve TPS/i 320 A model [21-22]

KR 8 R2100-2 arc HW Welding Robot		
Maximum reach	mm	2101
Maximum carrying capacity	kg	9,3
Payload	kg	8
Nominal additional load turnt able/connecting rod/lever	kg	0 / 0 / 10
Position repeat accuracy (ISO 9283)	mm	± 0,04
Number of axles		6
Installation area	mm	430,5x 370
Weight	kg	260
TPS/i 320 A Welding machine		
Maximum welding current	A	320
Minimum welding current	A	3
Welding current / Duty cycle [10min/40°C]	A	320 / 40%
Welding current / Duty cycle [10min/40°C]	A	260 / 60%
Welding current / Duty cycle [10min/40°C]	A	240 / 100%
Operating voltage	V	14.2-30
Open-circuit voltage	V	68
Mains frequency	Hz	50-60
Mains voltage [+/-15%]	V	3 x 400
Mains fuse	A	35
Size / Width	mm	300
Size/Length	mm	706
Weight	kg	33.7
Protection class	-	IP23

In Figure 4-a, connection of sample to be welded for temperature measurement with experimental setup is shown. Here, temperature is measured by technical K type thermo-couple from 4 different points. K type thermo-couples have been produced from NiCr-Ni alloy. Temperature measurement interval is between -200 and +1200 °C and voltage interval is between -5.891 and 54.807 mV.

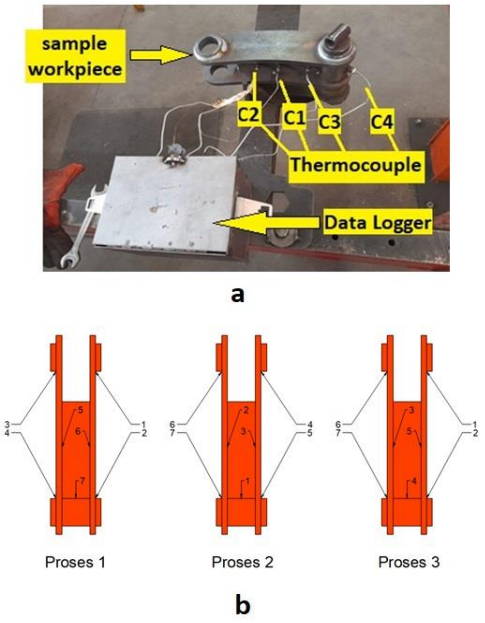

Fig. 4. Experimental setup (a), Welding sorting for each process (b)

While the experiments are carried out, 3 processes have been realised with different welding sorting. Moreover, after the start of welding process, temperature has been recorded for 3000s. Welding sorting of such processes are shown in the Picture in Figure 4-b by numbers. 3 sample parts have been used for each process in order to put forward validity of the experiment. In process number 1, welding sorting has been planned from outside to inside. The welding root takes position to weld firstly the welding lines no. 1 and 2. Then, welding is made in no. 3 and 4 in symmetry. Finally, no. 5, 6 and 7 are welded and the process is completed.

In Process number 2, a welding progress have been aimed from inside to outside. While the welding root takes position to weld firstly the welding lines no. 1, 2 and 3, welding is made in no. 4 and 5 afterwards. Finally, no. 6 and 7 are welded and the process 2 is completed. In process number 3, a welding progress have been aimed from right to left. The welding root completes circular the welding lines no. 1 and 2, and positions the workpiece in planar position and welds no. 3, 4 and 5. Finally, no. 6 and 7 are welded circularly and the process is completed. After the welding process, the parts are left for cooling.

During welding process, time-dependent temperature curves are formed. It has been observed according to the measured temperatures that the highest temperatures are between 250°C - 255°C. It has been observed at the end of 3000 seconds that the temperature of workpiece is around 50°C. Such temperature is not over the

room temperature.

Values obtained from temperature sensors have continued for 3000 seconds as of the initiation of welding process. Time-dependent graphics of temperatures of sample 1-1, 1-2 and 1-3 belonging to process 1 are shown in Figure 5. Here, the highest temperature has been measured as 255°C. It has been observed at the end of 3000 seconds that the temperature of workpiece is around 50°C. Moreover; it has been observed that the highest temperature in measurement points for 3 sample parts are in points 1, 2 and 3. The temperature at such points is around 250°C. The measurement point no. 4 differs from the others with a temperature of 150°C. At the end of the measurement, the temperature for 4 measurement points is approximately 50°C.

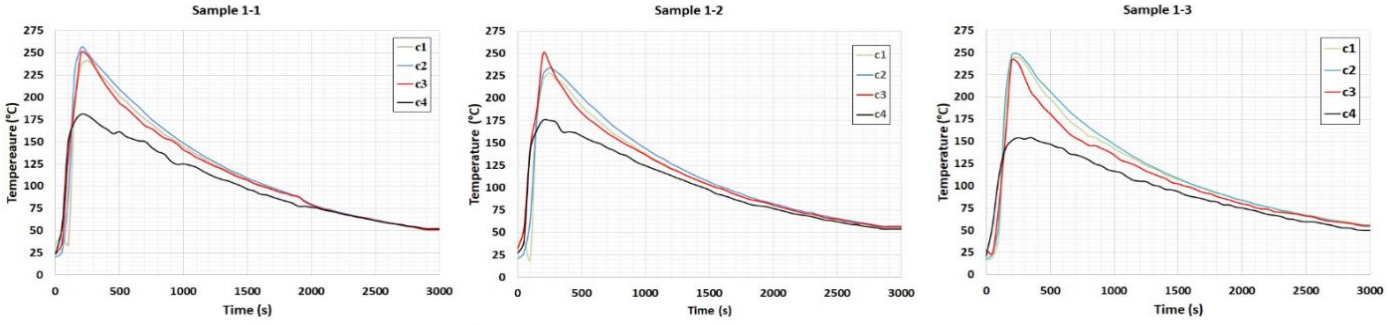

Fig. 5. Time-dependent graphic of 3 samples for Process 1

In Process 2, a welding process progressing outside to inside has been aimed. Time-dependent graphics of temperatures of sample 2-1, 2-2 and 2-3 belonging to process 2 are shown in Figure 6. Here, maximum temperatures at measurement points for each welded sample are balanced and close to each other. Maximum temperature value taken from the sensors is 220°C. At the end of the measurement, the temperature for 4 measurement points is approximately 50°C.

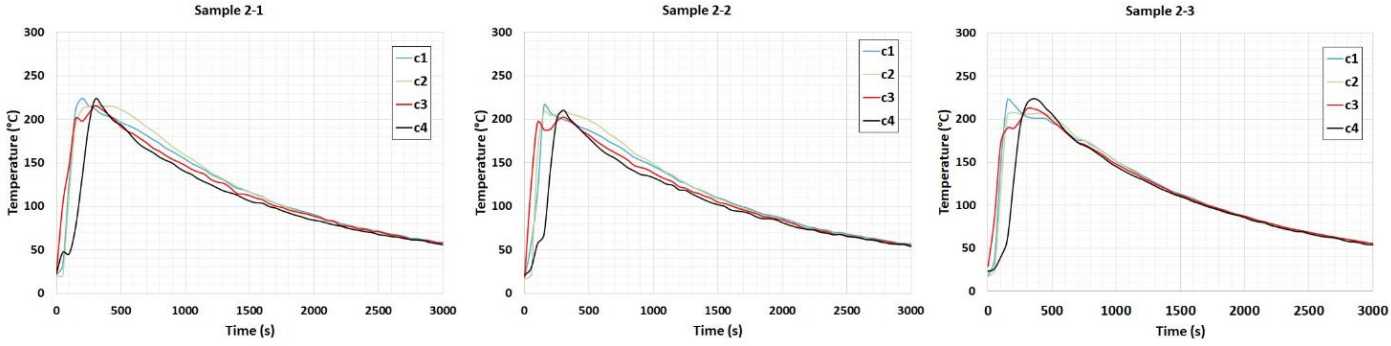

Fig. 6. Time-dependent graphic of 3 samples for Process 2

In Process 3, a welding process progressing right to left has been aimed. Time-dependent graphics of temperatures of sample 3-1, 3-2 and 3-3 belonging to process 3 are shown in Figure 7. Temperature curves in measurement points of Process 3 are similar to the process number 2.

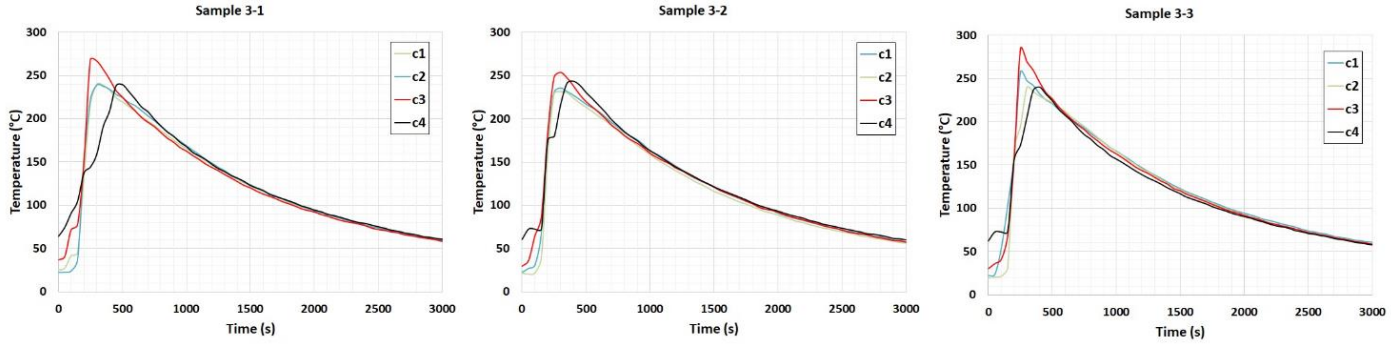

Fig. 7. Time-dependent graphic of 3 samples for Process 3

When temperature-time graphics are examined, it is observed that welding process is completed at lower temperatures in process 2. It has been observed that the temperature measure in C4 point is lower than the temperatures measured in other points in all processes. Especially in process 1, low temperature in C4 point is more distinctive.

3. Three-Dimensional Measurement Results

After completion of welding process, 9 samples belonging to 3 processes have been screened by laser screening device and three-dimensional models have been created. In Figure 8, displacements belonging to surfaces exposed to the highest number of displacements after welding processes are shown.

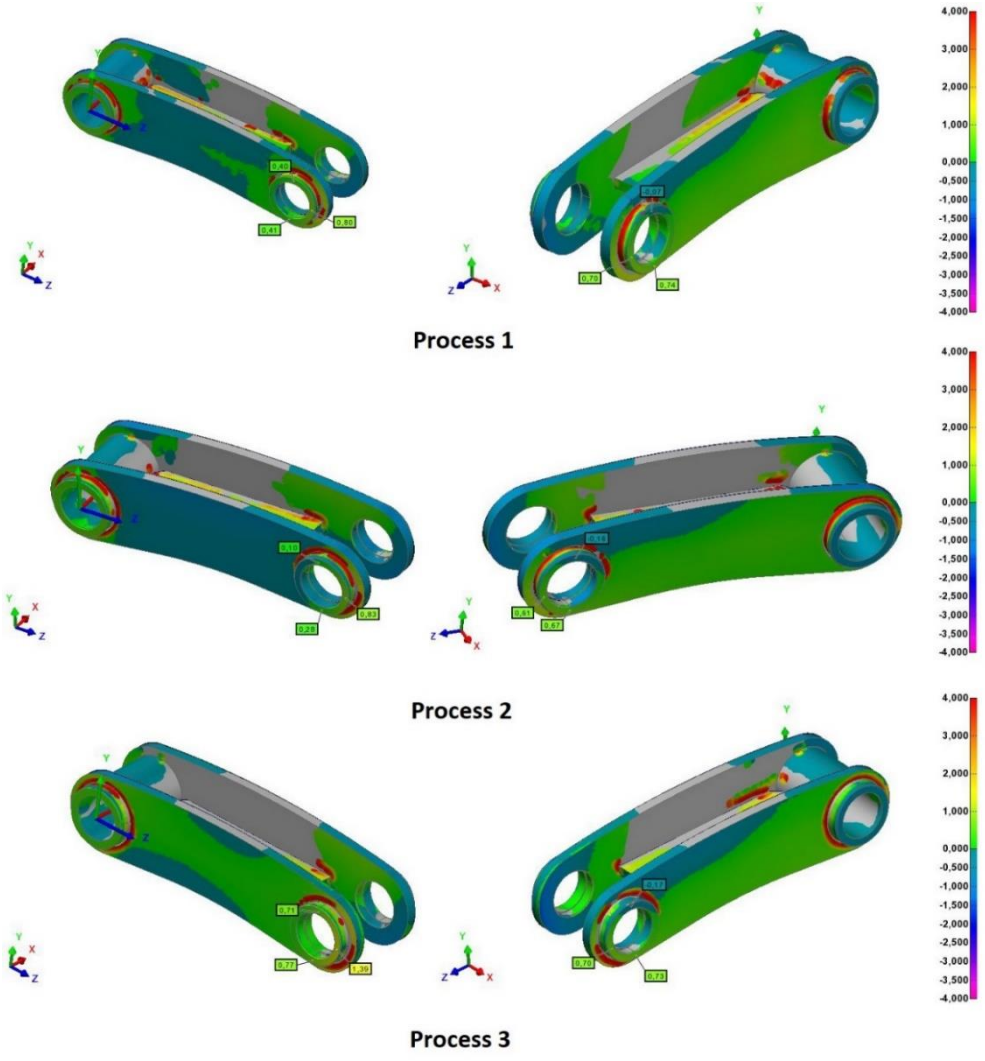

Fig. 8. Surface displacements measured by laser for all processes

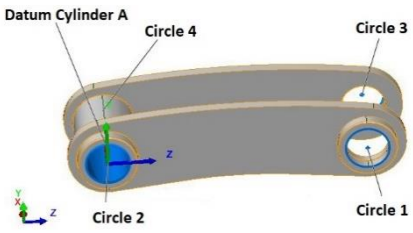

Fig. 9. Displacement areas on the part

When the figure is examined, displacements occurring in welding areas in all processes are evaluated as normal. However, when displacements on surfaces composing cylindric areas are examined, it can be said that the least amount of displacement has occurred in process no. 2 and the highest amount of displacement has occurred in process 3. ,

In Figure 9, displacements in cylindric and circular areas after welding are shown. Displacements in all processes have remained within tolerances. However, the least amount of displacements after welding has occurred in Process 2. In Table 3, ideal measurements and the displacements after welding process are shown.

Table 3. Displacement values of cylindric an circular areas on the part after welding process.

	Nominal		Process 1	Process 2	Process 3
	mm		mm	mm	mm
Datum cylinder A	42.35	**Measurement**	42.19	42.15	42.14
		Dev.	*-0.16*	*-0.20*	*-0.21*
Circle 1	42.35	**Measurement**	42.17	42.24	42.10
		Dev.	*-0.18*	*-0.11*	*-0.25*
Circle 2	43.15	**Measurement**	42.27	42.29	42.33
		Dev.	*-0.88*	*-0.86*	*-0.82*
Circle 3	42.35	**Measurement**	42.19	42.3	42.19
		Dev.	*-0.16*	*-0.05*	*-0.16*
Circle 4	43.15	**Measurement**	42.36	42.25	42.37
		Dev.	*-0.79*	*-0.59*	*-0.78*

Microstructure analysis is carried out by enlarging sections taken from the workpiece by 10x at maximum under the microscope and by cauterising with acid after being prepared metallographically. For corner welds in microstructure analysis, weld thickness, penetration, discontinuities are determined. Areas, where microstructure analysis has been carried out, are formed by taking sections shown in Figure 10. Macro image obtained from the welding area number 1 has been given in Figure 10-b. It has been observed that welding constrictor thickness of such area is 5.644. Penetration value is 1.645 mm for part 1; and 1.050 mm for part 2. Root penetration is 0.811 mm. The section taken from welding area number 2 is shown in Figure 10-c. Welding constriction thickness in such area is 5.245 mm; penetration value is 1.232 mm for part 1; and 1.220 for part 2. The section taken from welding area number 2 is shown in Figure 10-c. While welding constriction thickness is read for such area; it is observed that the root penetration value is 1.164 mm for part 1. Microscopic image of the welding are number 3 is shown in Figure 10-d. Welding constriction thickness in 5.716 mm; welding penetration is 1.145 mm for part 1, 1.145 mm for part 2. It has been observed that measurements of all samples are within acceptable limits.

4. Microstructure examination

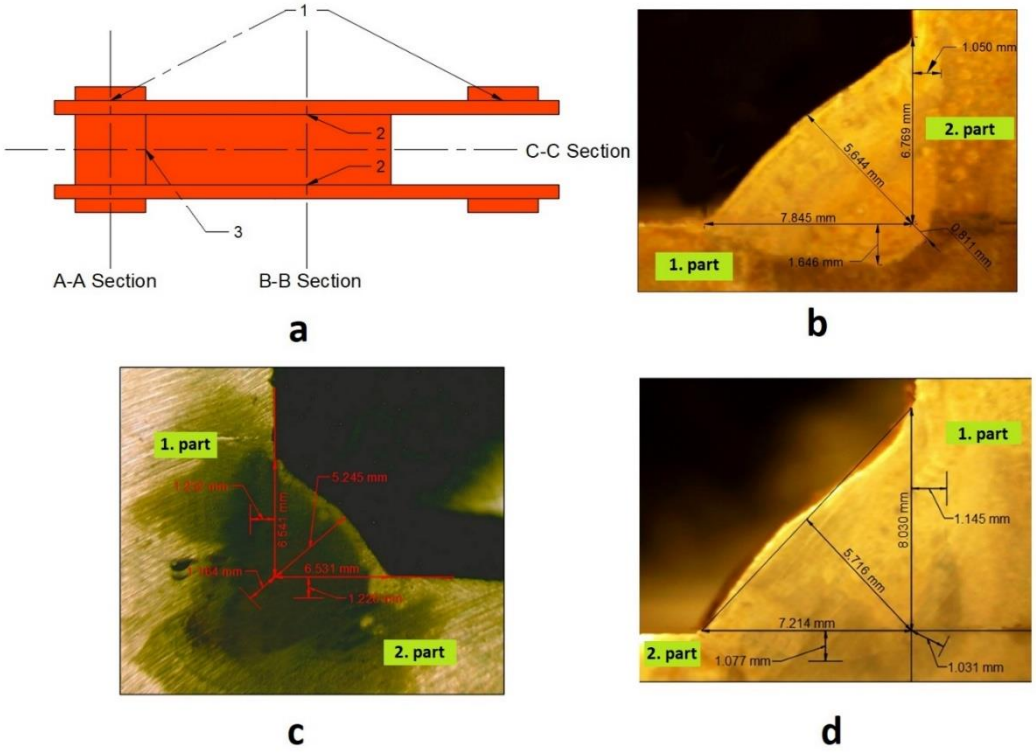

Fig. 10. Microstructure examination of welding areas. Section areas (a) welding of sections (b, c and d)

5. Conclusion and Suggestions

As a result of the measurements carried out, total cylindric and circular displacements are as process 2 (1.22 mm), process 3 (2,12 mm) and process 1 (2.17 mm) in ascending order. Lower amount of displacements in process 2, when compared to the others, results from occurrence of welding process at lower temperature.

Such situation prevents re-arrangement of the part or becoming unusable after the end of welding process. Maximum temperature values obtained from measurement points for the process number 1 at measurement points 1, 2, 3 and 4 are respectively as 270 °C, 265 °C, 380 °C ve 242 °C. Maximum temperature values obtained from measurement points for the process number 2 at measurement points 1, 2, 3 and 4 are respectively as 260 °C, 242 °C, 238 °C and 272 °C. Maximum temperature values obtained from measurement points for the process number 3 at measurement points 1, 2, 3 and 4 are respectively as 255 °C, 243 °C, 310 °C and 240 °C.

As a result of 3-dimensional measurements, maximum displacements of surfaces in process number 1 is respectively as 0.40 mm, 0.41 mm and 0.80 mm', 0.07 mm, 0.70 mm, 0.74 mm; in process number 2 as 0.10 mm, 0.28 mm and 0.83 mm, -0.16 mm, 0.61 mm, 0.67 mm; and in process number 3 as 0.71 mm, 0.77 mm and 1.39 mm, -0.17 mm, 0.70 mm, 0.73 mm. When such values are examined, displacement values of process 2 are lower than the others. Welding process at lower temperatures put forward positive results in displacements.

Penetration values for welding taken from workpieces are 1.232 mm for part 1 and 1.220 mm for part 2 in area number 1. Root penetration is 1.164 mm. In area number 2, it is 1.232 mm for part 1 and 1.220 mm for part 2. Root penetration is 1.164 mm. In area number 3, it is 1.232 mm for part 1 and 1.229 mm for part 2. Root penetration is 1.164 mm. According to related measurements, welding areas in all processes have compliant values.

Conflict of Interest Statement

The authors declare that there is no conflict of interest in the study.

CRediT Author Statement

Haluk Güneş **:** Conceptualization, Supervision

Salih Özdel **:** Conceptualization, Writing-original draft, Data curation, Formal analysis

References

[1] Kunt MA. An experimental investigation of exhaust waste heat recycling by thermoelectric generators under different thermal conditions for internal combustion engines. *Proceedings of the Institution of Mechanical Engineers, Part D: Journal of Automobile Engineering* 2017; 232: 1648-1653.

[2] Nart E, Celik Y. A practical approach for simulating submerged arc welding process using FE method. *Journal of constructional steel research* 2013; 84: 62-71.

[3] Yavuz N, Özcan R and Polat FG. Tozaltı kaynak bağlantısının sonlu elemanlar yöntemi ile termal ve mekanik analizi. *Uludağ University Mühendislik-Mimarlık Fakültesi Dergisi* 2005; 2: 9-19.

[4] Kaya F. Ark kaynak yöntemiyle birleştirilen çelik malzemelerin nümerik olarak modellenmesi. Master's Theses, Sakarya University, Türkiye, 2010.

[5] Wu A, Syngellakis S, & Mellor BG. Finite element analysis of residual stresses in a butt weld. In: The Post Graduate Conference in Engineering Materials Proceedings, University of Southampton. 2001.

[6] Wen SW, Hilton P, & Farrugia DCJ. Finite element modelling of a submerged arc welding process. *Journal of Materials Processing Technology* 2001; 119: 203-209.

[7] Gunaraj V, & Murugan N. Prediction of heat-affected zone characteristics in submerged arc welding of structural steel pipes. *Welding Journal* 2002; 81: 94-98.

[8] Song J, Peters J, Noor A, & Michaleris P. Sensitivity analysis of the thermomechanical response of welded joints. *International Journal of Solids and Structures.* 2003; 40: 4167-4180.

[9] Joshi S, Hildebrand J, Aloraier AS & Rabczuk T. Characterization of material properties and heat source parameters in welding simulation of two overlapping beads on a substrate plate. *Computational Materials Science* 2013; 69: 559-565.

[10] Piekarska W, Kubiak M. Modeling of thermal phenomena in single laser beam and laser-arc hybrid welding processes using projection method. *Applied Mathematical Modelling* 2013; 37: 2051-2062.

[11] Nezamdost MR, Esfahani MN, Hashemi SH & Mirbozorgi SA. Investigation of temperature and residual stresses field of submerged arc welding by finite element method and experiments. *The International Journal of Advanced Manufacturing Technology* 2016; 87: 615-624.

[12] Fachinotti VD, Cardona A, Baufeld B & Van der Biest O. Finite-element modelling of heat transfer in shaped metal deposition and experimental validation. *Acta materialia* 2012; 60: 6621-6630.

[13] Pu X, Zhang C, Li S, & Deng D. Simulating welding residual stress and deformation in a multi-pass butt-welded joint considering balance between computing time and prediction accuracy. *The International Journal of Advanced Manufacturing Technology* 2017; 93: 2215-2226.

[14] Knoedel P, Gkatzogiannis S & Ummenhofer T. Practical aspects of welding residual stress simulation. *Journal of Constructional Steel Research* 2017; 132: 83-96.

[15] Yadav A, Ghosh A & Kumar A. Experimental and numerical study of thermal field and weld bead characteristics in submerged arc welded plate. *Journal of Materials Processing Technology* 2017; 248: 262-274.

[16] Podder D, Mandal NR & Das S. Heat source modeling and analysis of submerged arc welding. *Welding journal* 2014; 93: 183-191.

[17] Minh PS, Phu TV. Study on the structure deformation in the process of gas metal arc welding (GMAW). *American Journal of Mechanical Engineering* 2014; 2: 120-124.

[18] Zhang J, Yu L, Liu Y, et al. Analysis of the effect of tungsten inert gas welding sequences on residual stress and distortion of CFETR vacuum vessel using finite element simulations. *Metals* 2018; 11:1-18.

[19] Çengel YA and Ghajar AJ. Heat Transfer A Practical Approach. İstanbul: Palme Yayıncılık, 2017, p.27.

[20] Eryürek İB. *Çelikler İçin Örtülü Elektrot Seçimi.* İstanbul: Kaynak

Tekniği Sanayi ve Ticaret A.Ş., 2007, p.11.
[21]Kuka smart automation systems, https://www.kuka.com/en-us/products/robotics-systems/industrial-robots/kr-cybertech-arc (2022, accessed 10 jun 2022).
[22]Fronius welding machine, https://www.fronius.com/en-us/usa/welding-technology/products/manual-welding/migmag/tpsi/tpsi/tps-320i (2022, accessed 10 jun 2022).

Nomenclature

CAE	: Computer Aided Engineering
FEA	: Finite Element Analysis
FEM	: Finite Element Method
HAZ	: Heat Affected Zone
MAG	: Metal Active Gas
MIG	: Metal Inert Gaz
TIG	: Tungsten Inert Gaz
ANN	: Artificial Neural Networks
Min	: Minute
°C	: Celsius
F	: Temperature factor
σ	: Stefan-Boltzmann constant
K	: Kelvin
A	: Ampe
V	: Voltage
C	: Karbon
Si	Silisium
Mn	Mangan
P	Phosphor
Ar	Argon
S	Sulphur
Al	Aluminium
ar	Rear length
af	front length
Hz	Hertz